Experiments in Fluids (2022) 63:106
https://doi.org/10.1007/s00348-022-03455-0

RESEARCH ARTICLE

Laboratory investigation of the near and intermediate wake of a wind turbine at very high Reynolds numbers

Alexander Piqué[1] · **Mark A. Miller**[2] · **Marcus Hultmark**[1]

Received: 6 October 2021 / Revised: 9 May 2022 / Accepted: 14 May 2022
© The Author(s), under exclusive licence to Springer-Verlag GmbH Germany, part of Springer Nature 2022

Abstract

The wake of a horizontal-axis wind turbine (HAWT) is investigated at very high Reynolds numbers, through a set of unique laboratory experiments. Well-resolved measurements of the axial component of velocity are performed using nano-scale hot-wire anemometry. The experiments were conducted at Reynolds numbers, based on the model diameter and free stream velocity, from 2.7×10^6 to 7.2×10^6, significantly higher than most previous laboratory studies. Measurements were acquired at five different downstream positions in the range of 0.77 to 5.52 diameters. It is shown that the Reynolds number effects on both the mean and fluctuating velocity fields are minor, and that the mean velocity exhibits self-similar behavior, but the variance does not. Analyses of the variance profiles, at different axial locations, are used to identify discrete tip vortices, and their locations, as well as an annular shear layer in the wake core rather than discrete root vortices. The existence of these structures is verified with phase averaged results.

Graphical abstract

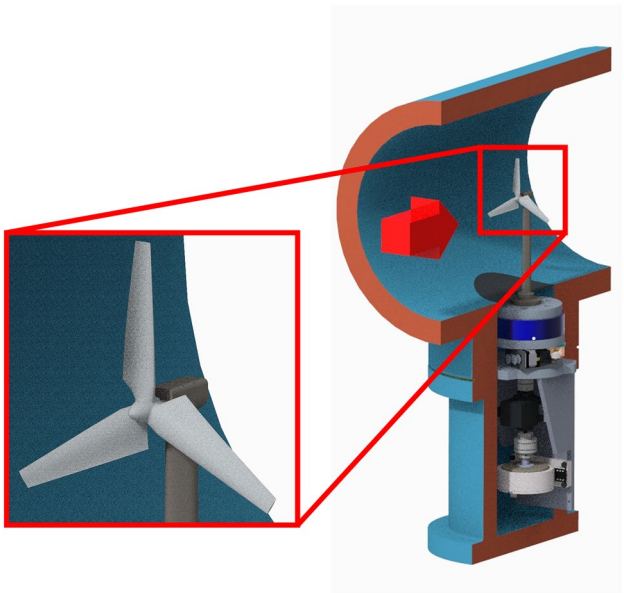

✉ Alexander Piqué
apique@princeton.edu

[1] Mechanical and Aerospace Engineering Department, Princeton University, Princeton, NJ 08544, USA

[2] Department of Aerospace Engineering, Pennsylvania State University, State College, PA 16801, USA

1 Introduction

In order to reduce land/sea installation costs of wind-farms, the spacing between wind turbines is unavoidably such that the wake of an upstream machine can affect one downstream. Since the wake behind a turbine has a

Published online: 10 June 2022

reduced flux of momentum compared to the undisturbed flow, the energy available for the downstream turbine to extract is reduced. A detailed understanding of how turbine wakes evolve and interact with downstream turbines is of great importance for improved wind farm planning and control. Modern horizontal-axis wind turbines (HAWTs) are characterized by their massive length scales, with modern rotors as large as 200 m in diameter. The large length scale is one factor that has made HAWTs successful, but is also what makes them particularly challenging to study in the field, laboratories, or numerically.

In general, turbine wakes can be divided into three regions: the near wake, the intermediate wake, and the far wake. In order to reduce computational and experimental costs, it is common to model a wind turbine wake as being generated by an axisymmetric and stationary drag generator, which eliminates the complex boundary conditions the rotating blades represent and the turbulent flowfield around them, which otherwise has to be calculated. For example, one such simplified representation of a HAWT is the commonly used actuator disk model, or equivalently a porous disk in experimental studies (Sforza et al. 1981; España et al. 2012; Howland et al. 2016). An underlying assumption in these simplified models is that the flow being modeled is that of the turbine's far wake, where the influence of the specific turbine geometry and blade-level details is not relevant.

The near wake is the flow region that is completely controlled by the initial conditions, such as the turbine geometry, resulting in tip vortices, and rotational effects (Vermeer et al. 2003). This region is often assumed to persist to at least a diameter downstream of the rotor. The intermediate wake serves as the bridge between the near and far wake, whereby the main flow characteristics are no longer dominated by the initial conditions and a transition to self-similarity has not yet been achieved. Self-similar behavior is the point at which properly nondimensionalized statistics collapse. It is also worth noting that the flow behavior in the intermediate wake is most relevant to turbine wake models as the typical turbine separation is normally less than 10 diameters, e.g., 5.8 diameters at the Nysted wind farm (Barthelmie and Jensen 2010) or 7 diameters at the Horns Rev wind farm (Gaumond et al. 2014). In addition, Meyers and Meneveau (2012) in an LES study showed that the ideal separation distance is 15 diameters. Therefore, an investigation of the differences between the near and intermediate wake of the studied turbine will be a theme of this study.

In the far wake, two different definitions are commonly used, one associated with classical turbulent wake theory and one in the wind energy community. In classical axisymmetric wake theory, the far wake is where the flow has "forgotten" the initial conditions and has achieved a universal self-similar behavior in the statistical moments. By this theory, the far wake is not expected to begin until 30 to 50 diameters downstream of the wake generator (Uberoi and Freymuth 1970; Johansson et al. 2003). Within the wind energy community, the far wake is commonly identified by the point at which the mean velocity deficit profiles obtain a Gaussian-like shape or the point at which any influence of the rotor has disappeared (Ainslie 1988; Vermeer et al. 2003). This interpretation is more closely related to the definition of the intermediate wake in turbulent wake theory. With this less stringent restriction, as compared with classical theory, the far wake of a turbine can be defined starting as early as three (Bastankhah and Porté-Agel 2014) or five (Chamorro and Porté-Agel 2009) diameters downstream.

The definition of the far wake commonly used in the classical turbulent wake literature will be used in order to make arguments on the self-similarity of the wakes presented in this study. Self-similar behavior in the statistical moments can provide valuable contributions to the wind energy modeling community. Wake models are used in wind farm layout tools and significantly affect the turbine spacing and layout. Increased understanding of the wake development downstream would lead to better models and more efficient wind farm developments. In addition, it is well known that inflow turbulence, whether due to the fluctuations in the atmospheric boundary layer or from the wake of an upstream turbine, has an effect on turbine performance (Lubitz 2014; Kamada et al. 2016; Talavera and Shu 2017). Therefore, an increased understanding of self-similar behavior in the velocity variance profiles can lead to more accurate models of turbines operating in the wakes of others.

If it is desired to replicate the turbine wake, consideration must be made regarding the matching of the most important non-dimensional groups governing the aerodynamics of a wind turbine between the field and model scales. These non-dimensional groups are the Reynolds number, $Re_D = U_\infty D\nu^{-1}$, and the tip speed ratio, $\lambda = \omega R U_\infty^{-1}$, where U_∞ is the freestream velocity, D and R are the rotor's diameter and radius, respectively, ω its angular velocity, and ν the kinematic viscosity. In order to accurately represent the aerodynamics of a wind turbine, in a simulation or experiment, both of these parameters need to be matched to field turbines. The Reynolds number of the largest turbines can be on the order of 10^8. The high Reynolds numbers alone represent a significant challenge for conventional laboratory-scaled tests, even in nonrotating cases, and to simultaneously match the tip speed ratio makes it significantly more challenging as they are inversely related to velocity. Only a few controlled laboratory studies, that are within an order of magnitude of the full-scale Reynolds numbers, have been performed. The National Renewable Energy Laboratory (NREL) Unsteady Aerodynamics Experiment (UAE) conducted experiments at Re_D up to 1.8×10^7, but these experiments did not take wake measurements (Butterfield et al. 1992; Robinson

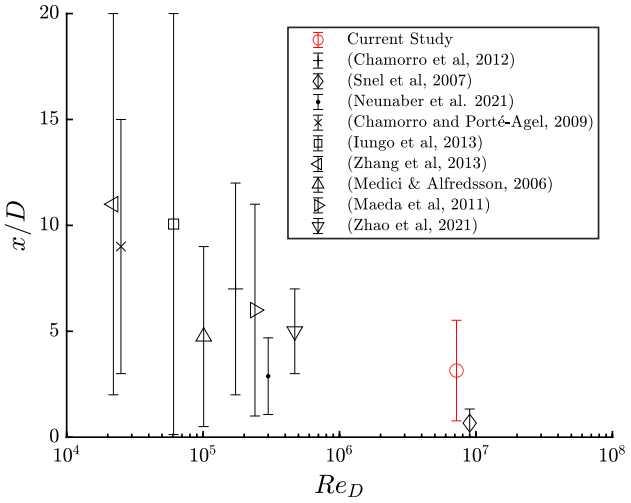

Fig. 1 Re_D and downstream range comparison of the current study, ○, to previous wind turbine wake experiments conducted within wind tunnel facilities: – (Chamorro et al. (2012)), ◇ (Snel et al. (2007)), • (Neunaber et al. (2021)), × (Chamorro and Porté-Agel (2009)),□ (Iungo et al. (2013)), ◁ (Zhang et al. (2013)), △ Medici and Alfredsson (2006), ▷ Maeda et al. (2011), ▽ Zhao et al. (2021)

et al. 1999; Simms et al. 2001). The Model Experiments in Controlled Conditions (MEXICO) project reached Re_D of nearly 9×10^6, but wake measurements only a little over a diameter downstream were acquired (Snel et al. 2007). A comparison of the maximum Re_D and downstream range of the presented study and a representative collection of past wind tunnel experiments, in which wind turbine wake data were acquired, can be found in Fig. 1. Immediately, it is clear that there is a lack of wake experiments conducted at high Reynolds numbers and over a sufficient range of downstream positions. The presented study fills this gap by introducing an experiment in which data at high Re_D are collected over a significantly larger range of downstream distances than any previous study. This enables investigations of high Reynolds number wake evolution.

It is often assumed that there exists a critical Reynolds number above which the non-dimensional statistics of the flow are independent of Reynolds number. However, there is little agreement over how high the Reynolds number needs to be for the aerodynamics of a wind turbine to reach such an invariant state, and if it extends to higher-order moments. To further complicate matters, Reynolds number effects play different roles when considering rotor performance, in the form of the thrust coefficient ($C_T = T\left(0.5\rho A U_\infty^2\right)^{-1}$) and the power coefficient ($C_P = P_t\left(0.5\rho A U_\infty^3\right)^{-1}$), or the wake itself. Here, P_t is the power produced by the turbine, A is the area swept by the turbine, ρ is the fluid density, and T is the thrust force. When considering the axial induction factor and in turn C_T, Sørensen et al. (1998) argued in a numerical study of an actuator disk that the Re_D limit could be as low as 2000. When considering C_P, Miller et al. (2019) determined that a far greater Reynolds number was needed for invariance. For the studied turbine, the rotor's C_P did eventually achieve Reynolds number invariance that was best characterized by a blade-level Reynolds number of $Re_c = 3.5 \times 10^6$, where the only effect of tip speed was to set the local tip velocity. This corresponded to large Re_D values, for example, at $\lambda = 7$ the requisite diameter

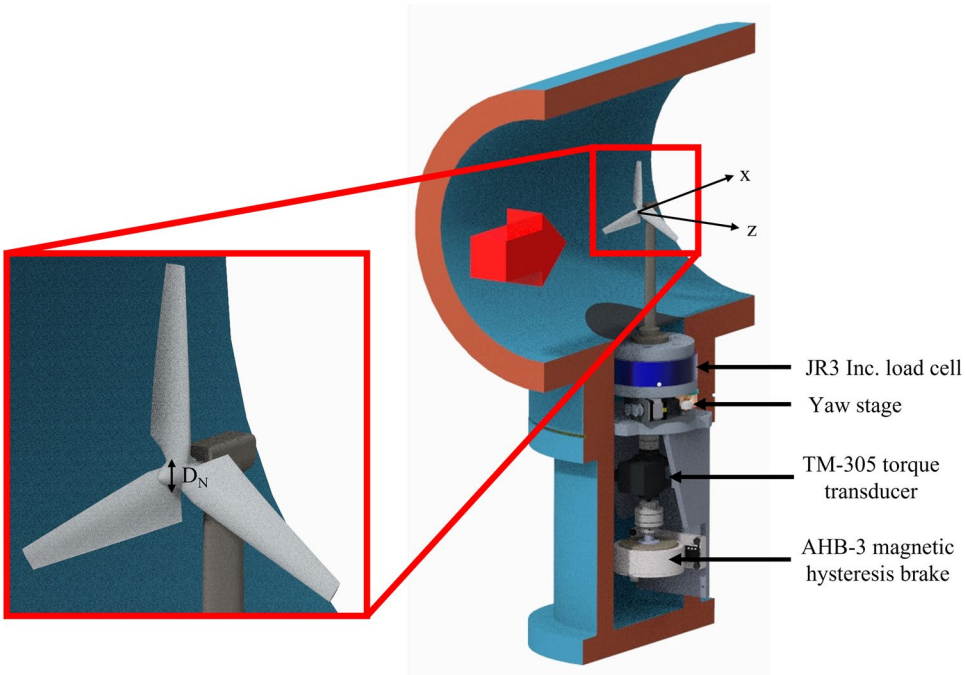

Fig. 2 Turbine measurement stack in HRTF and coordinate system of wake measurements. The large red arrow indicates the direction of flow. The diameter of the turbine's nacelle, D_N, is 0.0146m

Reynolds number for invariance was $Re_D \approx 8 \times 10^6$. When considering the turbine's wake, Chamorro et al. (2012) showed evidence of a collapse of turbulence statistics at Re_D=9.3×10^4. Meanwhile, McTavish et al. (2012) showed that the wake expansion and tip vortex location were still evolving beyond that Reynolds number. Tip vortices are signatures of the rotor and will be found in the near wake, a region expected to be affected by Reynolds number (Wang et al. 2021). In addition, the transition to self-similarity requires studying the evolution of higher-order statistical moments, as well as potential Reynolds number effects. Previous research of other axisymmetric wake generators has shown that self-similar behavior for higher-order moments requires a greater downstream distance and higher Reynolds numbers (Johansson and George 2006; Jiménez et al. 2010). To summarize, multiple thorough attempts have been made to understand the effect of Reynolds number on wind turbine wakes. However, the limited number of high Reynolds number experiments makes it difficult to validate any invariance or trends determined from measurements obtained at lower Reynolds numbers.

The present study was designed to address some of the open questions on the scaling of the near and intermediate wake at some of the highest Reynolds numbers ever tested in a laboratory environment for a wind turbine wake. Initial results for this setup were first presented in Piqué et al. (2020), but they were limited to a discussion on Reynolds number invariance and a brief discussion on the possibility of wake meandering being present in the turbine's wake as represented by a Strouhal number, $St = 0.3$. The study presented here will expand on the initial investigation with comments on self-similarity and the identification of periodic structures. A more detailed investigation of the wake structures will be the topic of a future study. The wakes of a model-scale wind turbine were acquired using nano-scale hot-wire anemometry at $2.7 \times 10^6 < Re_D < 7.2 \times 10^6$. Across all wake measurements, the tip speed ratio was kept constant, $\lambda = 5.54 \pm 0.11$. This tip speed ratio corresponds with a point near the turbine's maximum power production, $C_{P,max}$ (Miller et al. 2019). Measurements were acquired in the wake at $-0.81 < z/D < 0.81$ on a horizontal plane at downstream distances of $0.77 < x/D < 5.52$. The downstream extent of the measurements was limited due to the expected interaction between the tunnel walls and the expanding wake. The authors have chosen to focus in particular on the near to intermediate wake due to the importance of this region to wind farm layout. Conclusions on wake evolution are made through a discussion on the presence of self similar behavior in the mean axial velocity deficit and variance profiles. Phase averaged results are used to validate the presence of dominant structures.

2 Experimental setup

2.1 Flow facility and wind turbine model

The data presented herein were acquired in the High Reynolds number Test Facility (HRTF) at Princeton University. The HRTF is a closed-loop wind tunnel that uses dry compressed air, up to 238 atm, as the working fluid. The high pressure enables tests at high Reynolds numbers without the need of large models and high velocities. A 149 kW motor is used to propel the compressed air up to 10 m/s, although the freestream velocities in this study were always below 5 m/s (detailed test conditions for a series of experiments conducted at $x/D = 0.77$ can be found in Table 1). Before reaching the test section, the flow is conditioned, which yields a uniform velocity field with axial turbulence intensities ranging from 0.51% to 0.73% for the lowest and highest Re_D tested in this study, respectively. These inflow conditions are not representative of what a wind turbine in the field would be exposed to, which would include shear, veer, stability and other complicating factors. However, by studying idealized and well-controlled inflow conditions, it is possible to decouple inflow effects from true Reynolds number effects on the aerodynamics and wake dynamics. Furthermore, the canonical inflow conditions make the data presented herein valuable as a reference data set.

The 4.88 m long test section has a circular 0.49 m diameter cross section with a 0.25 m diameter access port, located on top of the test section. The access port was used to mount the turbine assembly and house its measurement stack such that it was kept outside the test section but inside the high-pressure environment. Electrical connections for the traverse and hot-wire anemometry system were fed through a 0.1 m diameter access port located on the bottom of the test section. For more information about the HRTF please see Jiménez (2007); Miller et al. (2019).

The model turbine used in this study features NACA 6 series airfoils and is 0.2 m in diameter. For the range of $0.074 < z/D < 0.5$, the airfoil geometry consisted of a NACA63-235 at the root and a NACA63-214 at the tip. The airfoil geometry between the tip and the root consisted of a swept blend between the root and tip airfoil geometries. The pitch is fixed at 5°and is defined positive in the direction of the oncoming flow from the rotor plane. The twist angle at the root is 13°. The chord length at the blade tip is 11.11mm, and the chord length at the root is 28.89mm. The rotor is identical to that used by Miller et al. (2019). CAD files of the tested rotor and tower assembly can be found in the public repository listed at the end of this manuscript. The transmission assembly was completely housed within a custom turbine tower. The rotor was mounted to a drive shaft, and the mechanical energy was transmitted through a 1:1

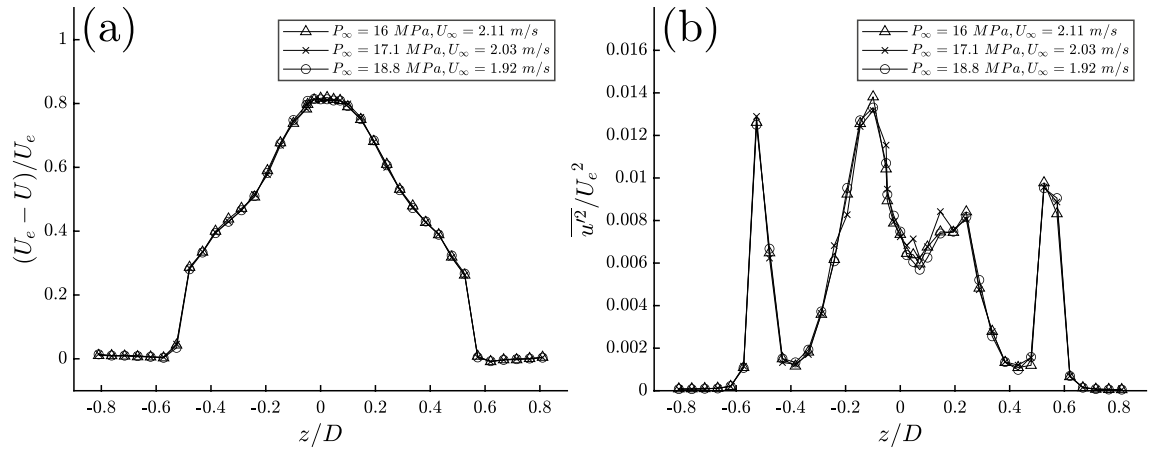

Fig. 3 Self-similar behavior of mean axial velocity deficit (a) and variance (b) profiles with changing static pressure, P_∞, and freestream velocity, U_∞, at $Re_D = 3.6 \times 10^6$ and $x/D = 0.77$. For this study of static pressure and freestream velocity invariance, 39 spanwise measurements were taken. The pressure range of the profiles displayed covers the approximate range over which all experiments were conducted

Table 1 HRTF flow conditions for presented wake experiments at $x/D = 0.77$. P_∞ is equivalent to the tunnel static pressure. The measured C_T and C_P values have been corrected for blockage ($C_{T,c}$ and $C_{P,c}$, respectively) following Bahaj et al. (2007). As can be seen in the table, the C_T values differ by more than 10%, but this can be expected to be due to the experimental uncertainty mentioned in (Miller et al. 2019) due to the use of a load cell with a resolution of $\pm 2.5N$. Uncertainty in the C_T measurements ranged from 6.09% for the highest Re_D case to 41.8% for the lowest Re_D case

Re_D	P_∞ (MPa)	U_∞ (m/s)	λ	C_T	$C_{T,c}$	C_P	$C_{P,c}$
2.7×10^6	18.7	1.42	5.61	0.896	0.788	0.422	0.349
3.6×10^6	18.6	1.91	5.56	0.823	0.735	0.431	0.364
4.5×10^6	18.6	2.42	5.49	0.823	0.735	0.427	0.361
7.2×10^6	16.7	4.23	5.58	0.789	0.708	0.393	0.334

miter gear assembly. In addition, the turbine was not driven by an external motor, but was self-starting. The self-starting nature of the turbine limited the lower bound of the Reynolds number operating range. In addition, at lower Reynolds numbers, the rotational speed of the turbine was reduced to ensure tip speed ratio matching. At low shaft torques, the losses present in the drive train are too great to accurately measure the aerodynamic rotor torque. Also, experiments at higher Reynolds numbers ran the risk of miter gear failure, limiting the upper bound of the Reynolds number operating range. Another drive shaft transmitted the mechanical energy down the length of the tower and to the measurement stack. The drive shaft interfaced with an in-line torque transducer (Magtrol Inc. model TM-305) that measured the instantaneous torque generated by the turbine and its rotational speed. The torque transducer interfaced in-line with a magnetic hysteresis brake (Magtrol Inc. model AHB-3) that was used to control the rotational speed and hence λ. Despite a constant brake load imposed by the hysteresis brake, small changes in fluid properties over the course of a wake measurement caused changes in the turbine's rotational speed; however, changes in λ never exceeded 1.39%. All in-line connections were facilitated by Zero-Max flex couplings. The turbine tower was secured to a 1000 N load cell (JR3 Inc.) that collected the force measurements in all three dimensions and moment measurements along all three axes. Torque data from the torque transducer were processed through an on-board 40 Hz low-pass filter and data from the force sensor were collected at 1000 Hz. Data from these two transducers, along with freestream velocity and density, are used to calculate C_P and C_T of the turbine. Freestream velocity was measured by a pitot-static tube that was mounted 0.74 m upstream of the turbine, and fluid density was found with real gas relationships using measurements of the static pressure and temperature inside the HRTF. The pressure and temperature measurements were made using an Omega PX419 sensor and a resistance temperature detector (Omega Technologies Corporation), respectively. Due to the very high Reynolds numbers of the experiments, the boundary layers present on the tunnel walls are expected to be very thin. Therefore, any streamwise pressure gradient effects due to them will also be very small. The performance metrics of

the turbine were not a focus of this study, as previous studies have extensively investigated the performance of this rotor and the role of Reynolds number (Miller et al. 2019). The coordinate system used throughout this study is shown in Fig. 2, where x denotes the axial direction, z is the spanwise direction and the origin is at the center of the rotor. The turbine rotates clockwise when viewed from the front.

To validate the setup and estimate experimental errors, the same test cases (non-dimensionally) can be achieved using different combinations of static pressure and freestream velocity. Dynamic similarity of the flow implies that the results should be identical, when non-dimensionalized appropriately. One such test is shown in Fig. 3, where three tests collapse almost perfectly when reduced by the free stream velocity outside of the wake at the downstream location, U_e.

2.2 Instrumentation

Hot-wire anemometry was used to acquire velocity data in the wake of the turbine and has been used by many previous studies to study the wake and its structures (Medici and Alfredsson 2006; Chamorro and Porté-Agel 2009; Chamorro et al. 2012; Iungo et al. 2013; Zhang et al. 2013; Piqué et al. 2020; Wang et al. 2021). However, achieving high Reynolds numbers in small-scale experiments yields reduced turbulent length scales, which can result in spatial filtering using conventional sensors. To reduce spatial and temporal filtering, the nano-scale thermal anemometry probe (NSTAP) was used for all velocity measurements in the wake. The NSTAP is fabricated in-house using standard micro-electromechanical system (MEMS) techniques. It features a freestanding 60 μm × 2 μm × 100 nm platinum sensing element supported by a silicon structure (Vallikivi et al. 2011; Fan et al. 2015). Measurements of the spectra were used to estimate the Kolmogorov length scale and found to be 10.5 μm, at the highest Reynolds number tested. With the longest dimension of the NSTAP being 60 μm, only minimal spatial filtering is expected. The reduced size of the sensing element not only reduces spatial filtering, but the small thermal mass increases the bandwidth as well (Hutchins et al. 2015). The NSTAP was operated in constant temperature mode using a Dantec Streamline CTA circuit. The measured NSTAP square wave response was approximately 200 kHz in this configuration. The NSTAP was calibrated in situ against a pitot tube which was located 199 mm from the turbine centerline, on the side opposite of the turbine tower, well outside of the wake. Calibrations of the NSTAP were performed before and after acquisition of each wake profile, at nine free-stream velocities with the NSTAP located outside of the wake and a fourth-order polynomial curve-fit was applied. Since temperature changes were always less than 1.28°C between calibrations, temperature corrections were not applied to the velocity measurements. In addition, conducting calibrations before and after data collection indicated negligible differences between pre- and post-calibrations. The error in the velocity measurements, based on the maximum difference between the pre- and post-calibration datasets, was less than 0.44%.

A four-axis traverse was used for controlling the NSTAP's position in the turbine wake. Spanwise velocity profiles were acquired on a plane perpendicular to the turbine tower and parallel to the rotor's center-axis. Five different downstream locations were sampled at $x/D = 0.77, 1.52, 2.02, 3.52$ and 5.52. As mentioned before, these downstream positions were expected to adequately encompass the near and intermediate wakes of the tested turbine. 81 spanwise measurement points were sampled at the closest downstream position, and 39 points were sampled at all other downstream positions. Additional spanwise points were collected at $x/D = 0.77$, so that phase averaging could be used to identify vortical structures, whose formation is dependent on the unique geometry of the tested turbine. At each spanwise point, velocity measurements were acquired for at least 200 turbine rotations (600 tip vortex passages) to ensure converged statistics up to the second moment. Comparisons to previous wake measurements will not be made because of the unique turbine geometry used in this study and the previously discussed effects of rotor geometry on the near wake (Kang et al. 2014; Howard et al. 2015; Abraham et al. 2019).

3 Results and discussion

3.1 Self-similarity of the mean axial velocity

Classical turbulent wake theory suggests that the characteristic velocity and length scales are the maximum deficit velocity ($u_0 = U_e - U(z = 0)$), and the wake half-width (l_0), respectively (Townsend 1956). The half-width is the spanwise distance from the centerline at which the velocity deficit is equal to $\frac{u_0}{2}$. Here, to account for blockage in the experimental setup (16.7%), U_e is taken as the mean velocity outside of the wake at the evaluated downstream location. In addition, the authors refer the reader to Figs. 5 and 6 for axial velocity deficit and variance profiles, respectively, that are nondimensionalized using U_e and D, more common scaling methods in the wind community. However, since the focus of this study is on self-similarity, the analysis and discussion will focus on the profiles nondimensionalized by conventional scaling methods, such as u_0 and l_0. Figure 4 shows the downstream evolution of the average deficit velocity profiles, non-dimensionalized with the wake length and velocity scales for $Re_D = 2.7 \times 10^6$ and 7.2×10^6. There is a convincing collapse of the profiles for $x/D \geq 1.52$

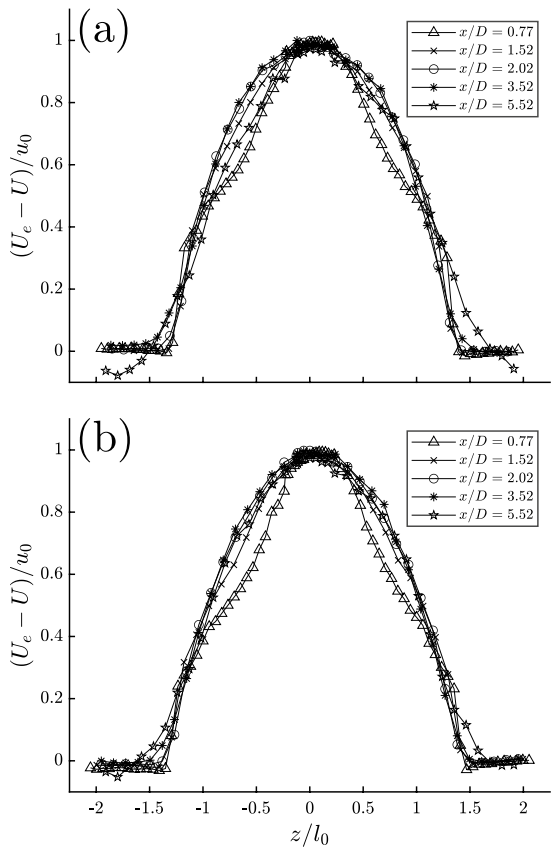

Fig. 4 Mean velocity deficit profiles at $Re_D = 2.7 \times 10^6$ (a) and at $Re_D = 7.2 \times 10^6$ (b)

for both Reynolds numbers. For the closest test location at $x/D = 0.77$, the profile does not collapse with those at the other downstream locations, indicating that the mean velocity has not yet reached self-similarity. As such, memory of the rotor therefore persists to at least $x/D = 0.77$.

The collapse of the mean velocity profiles for $x/D \geq 1.52$ is a potential indicator of a transition out of the near wake. However, higher-order moments are known to evolve more slowly than the mean and may still be subject to initial conditions determined by the rotor geometry. A study of the variance will shed more light as to when the main turbine-dependent flow structures of the near wake, such as the tip vortex, have decayed. Only once these flow signatures have decayed can the wake be considered to have transitioned out of the near wake. Previous turbine wake studies have made similar conclusions regarding a rapid transition to a self-similar mean velocity profile, with typical distances between 3-5 diameters (Chamorro and Porté-Agel 2009; Bastankhah and Porté-Agel 2014).

In addition to studying the near-to-intermediate wake transition, Reynolds number effects on wake recovery were also investigated. Velocity deficit profiles nondimensionalized by U_e and D are shown in Fig. 5 across the Re_D tested. A convincing collapse across the Re_D range for all downstream positions is found, except for $x/D = 5.52$. At $x/D = 5.52$, no discernible trend can be found to explain the lesser degree of collapse for this position when compared to the $x/D < 5.52$. However, the lack of collapse may be due to a relative increase in error as a result of the decreasing deficit velocity with increasing downstream distance.

3.2 Downstream evolution of the velocity variance profiles

To evaluate the wake evolution, the existence of rotor-dependent flow structures, and the transition from the near wake, the behavior of the second-order moment of the axial velocity is investigated. A better understanding of the turbulent fluctuations in the wake is also of great interest when considering turbine placement in a wind farm, where the wake of one turbine acts as the inflow to a downstream

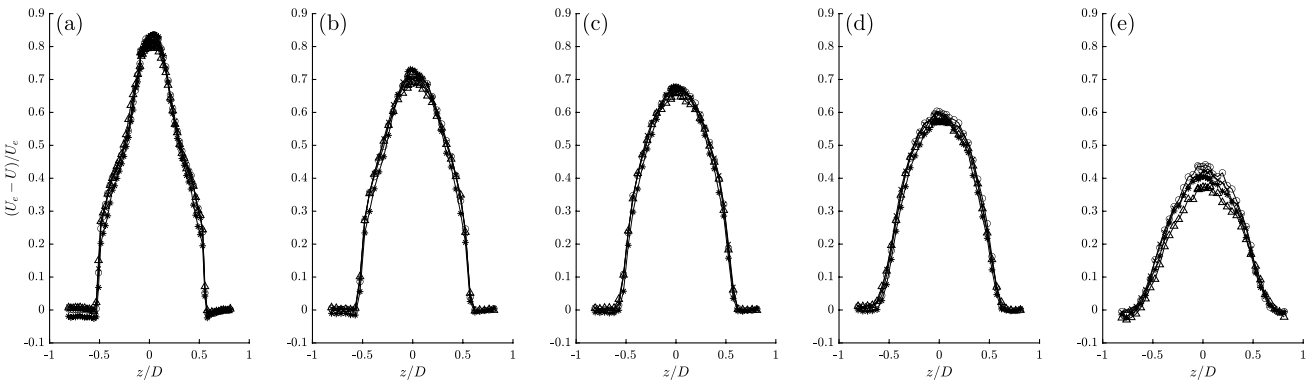

Fig. 5 Mean velocity deficit profiles nondimensionalized by U_e and D to illustrate wake recovery across all downstream positions, $x/D =$ 0.77(a), 1.52(b), 2.02(c), 3.52(d), 5.52(e) across all Reynolds numbers tested ($\triangle$, $Re_D = 2.7 \times 10^6$, $\times$, $Re_D = 3.6 \times 10^6$, $\circ$, $Re_D = 4.5 \times 10^6$, $*$, $Re_D = 7.2 \times 10^6$)

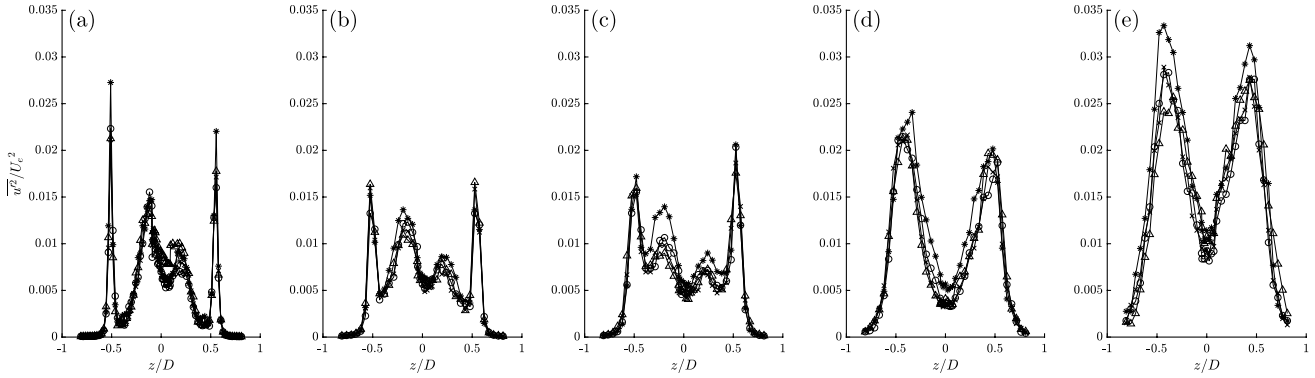

Fig. 6 Axial variance profiles nondimensionalized by U_e and D across all downstream positions, $x/D = 0.77$(a), 1.52(b), 2.02(c), 3.52(d), 5.52(e) across all Reynolds numbers tested ($\triangle$, $Re_D = 2.7 \times 10^6$, $\times$, $Re_D = 3.6 \times 10^6$, $\circ$, $Re_D = 4.5 \times 10^6$, $*$, $Re_D = 7.2 \times 10^6$)

turbine. Figure 7 shows the downstream evolution of the non-dimensionalized variance of the axial velocity. By scaling in this manner, it is difficult to visualize the axial variance profiles for $x/D \leq 2.02$. For this reason, the variance profiles for $x/D \leq 2.02$ are also depicted in Fig. 8.

For $x/D \leq 2.02$, the variance profiles are characterized by two narrow "outer" peaks near the edge of the wake, which are likely signatures of the tip vortices, and two smaller "inner" peaks located near the center that could be signatures of the root vortices. Similar axial variance features have been found in previous experimental works at much lower Reynolds numbers and have been used to identify the tip and root vortices (Maeda et al. 2011; Odemark and Fransson 2013). The outer peak location is in the region of $1 < |z/l_0| < 1.5$, and the inner peak location is in the region of $0.25 < |z/l_0| < 0.75$. However, local areas of high variance are not necessarily evidence of discrete vortices, but could also indicate regions of intense mixing, such as in a shear layer.

With increasing downstream distance, the nondimensionalized outer peaks grow in both width and magnitude, as shown in Fig. 7. The widening of these peaks is consistent with tip vortex breakdown as the once coherent structures are being diffused due to interactions with other vortical structures and momentum transfer between inner and outer wake flow. In the region between $2.02 < x/D < 3.52$, the wake transitions from a four-peak behavior in the variance profile to a two-peak behavior. Previous research has suggested that the tip vortices and the root vortex interact in a destructive manner so that their periodic behavior is destroyed and replaced by a single annular shear layer (Foti et al. 2016). The two-peak profile observed at $x/D \geq 3.52$ suggests that the wake is defined by an annular shear layer, similar to a wake generated by a non-rotating body. Another conclusion that can be made is that self-similarity in the variance profiles is not obtained for any of the downstream positions tested.

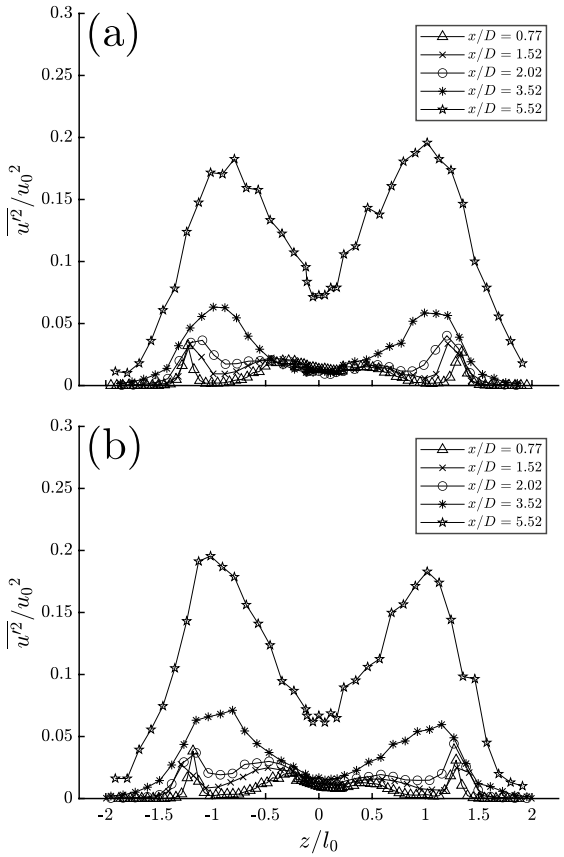

Fig. 7 Axial variance profiles at $Re_D = 2.7 \times 10^6$ (a) and at $Re_D = 7.2 \times 10^6$ (b)

Earlier, it was hypothesized that the near wake transitioned to the intermediate wake somewhere in the region $0.77 < x/D < 1.52$, due to the collapse of the mean profiles for $x/D \geq 1.52$. However, the variance profiles suggest that the near wake extends to somewhere between

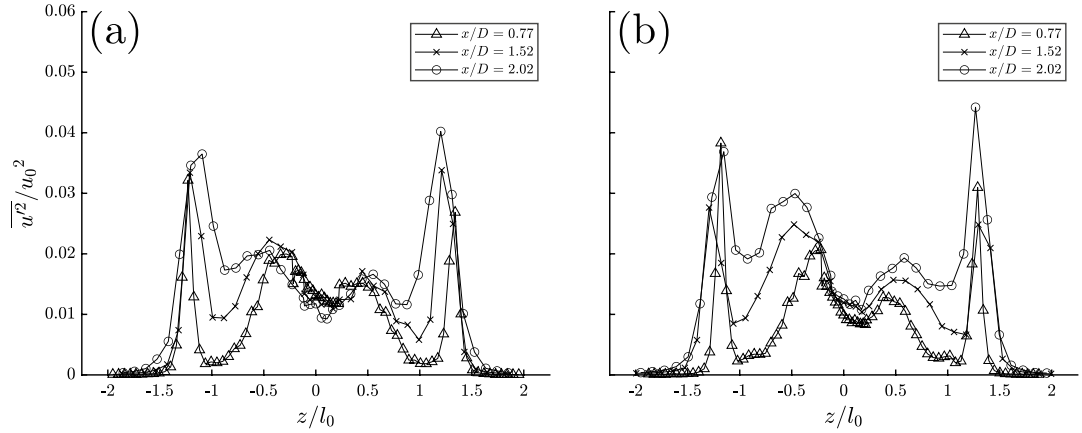

Fig. 8 Axial variance profiles for the near wake ($x/D \leq 2.02$) for $Re_D = 2.7 \times 10^6$ (a) and 7.2×10^6 (b)

$2.02 < x/D < 3.52$, as the strong presence of the inner and outer peaks is present for locations upstream of $x/D = 3.52$. This transition region from the near to the intermediate wake is also affected by the low turbulence intensity inflow conditions of the HRTF. The observed behavior with self-similarity in the mean velocity deficit, but not in the variance profiles at the same downstream position, has been seen in other axisymmetric wake flows (Jiménez et al. 2010; Dairay et al. 2015). The collapse of the inner and outer peaks profiles and the transition to an annular shear layer in the flow region of $2.02 < x/D < 3.52$ is evident from the variance profiles shown in Fig. 7, suggesting that a transition to the intermediate wake occurs in that region. From this discussion, by the wind energy community assumption, the far wake would be defined as starting somewhere in the region of $2.02 < x/D < 3.52$, because in this region, the vortical structures unique to the rotor, specifically the tip vortex, have broken up.

As can be seen in the near wake depicted in Fig. 8, the outer peaks do not collapse, whereas the inner peaks seem to collapse fairly well in the region $-0.5 < z/l_0 < 0.5$, especially at the lower Reynolds number. For the high Reynolds number, Fig. 8b, there is some evidence of collapse near the core, but the spanwise extent is less than at the lower Reynolds number, 8a. The observed local collapse in the wake core is somewhat surprising due to expected strong interactions between the vorticity shed across the blade's span. The collapse at the core of the wake suggests that it might not be dominated by discrete vortical structures solely generated at the turbine's root, but that the root may be producing an annular shear flow, which could be the signature of hub and root vortices that had been broken up further upstream. In addition, a strong level of asymmetry can be observed for the inner peaks. At this time, the authors do not have an explanation for the observed phenomenon. A slight misalignment of the turbine could explain the asymmetry in the variance, as has been observed in, for example, Lin and Porté-Agel (2019), but no evidence of misalignment of the turbine can be found in the symmetric deficit profiles. It is also possible that the presence of the tower, which breaks the axisymmetry of the setup, can contribute to the observed asymmetry.

4 Validation of dominant vortical wake structures

In Sect. 3.2, it is indicated that the near wake is populated by discrete tip vortices in the tip area, given the large variance peaks at the wake edge. It is further indicated that the wake core does not contain discrete root vortices, but instead is characterized by a shear layer. To verify these observations, phase averaging was conducted under the assumption that the phase period was equal to the turbine rotation period, T_{rot}, which provides insight as to the extent that the wake flow is affected by a periodic motion with a frequency equal to the turbine's rotation rate.

The experimental setup did not include an absolute position encoder for the turbine, meaning the location of a certain turbine blade was unknown during the experiment. However, it was expected that the vorticity shed from an individual turbine blade would interact with the tower as it passes, leading to a periodic signal in the streamwise force (Fontaine et al. 2020). Spectra of the streamwise force signal confirmed this expectation because the signal had a dominant periodic signal equal to $3f_{rot}$. The time signal of the first blade passing in the force signal was used to initiate the velocity data set that would be phase averaged. Following the bin phase averaging method discussed in Sonnenberger et al. (2000) and using 4000 bins per period, the remaining

velocity data set was divided up into periods based on the average turbine rotation rate for that spanwise location.

Phase averaged results of the axial velocity data at $x/D = 0.77$ for Re_D=2.7×10^6 and 7.2×10^6 are shown in Fig. 9. If discrete root vortices were present, there should be at least three regions of high and low velocity in the wake core. From Fig. 9, there is no sign of an alternating velocity signal in that region of the wake, thus supporting the conclusion that the wake core is populated by a shear layer, and that any memory of discrete root vortices is gone already at $x/D = 0.77$. The coherent core of low velocity, ($|z/D| \leq 0.2$), also suggests that there is a small amount of wake recovery between the core and the external flow in the near wake. Accuracy of any observed length scales associated with the tip vortices is limited due to the spanwise resolution of the sample sites (0.0231D), which is comparable to the tip vortex size. To probe the core region in the near wake, the spanwise gradients of the mean velocity deficit profiles at $x/D = 0.77$ are shown in Fig. 10a.

At $-0.6 < z/D < -0.45$, a large and sudden change in the magnitude of the spanwise gradient is observed in Fig. 10a. This sudden change in spanwise gradient is an indicator of the tip vortex. However, near the center, at $z/D = -0.2$, there is another local maximum in the spanwise gradient, albeit smaller than that at the wake edge. This is consistent with the core acting like a wake within the wake and that the root vortices must have already broken up. This flow feature can be pictured as the wake produced by the turbine's hub and root and is likely a unique flow feature for the studied turbine. The coexistence of two wakes suggests that the wakes produced by the turbine and the hub are characterized by different scales. The turbine wake dominates the span and is characterized by the turbine's diameter. The "hub wake" is characterized by a smaller length scale, which also explains the more rapid transition to self-similarity observed in the core region of the axial variance profiles. A potential different characteristic length scale of the "hub wake" will be the subject of a future study.

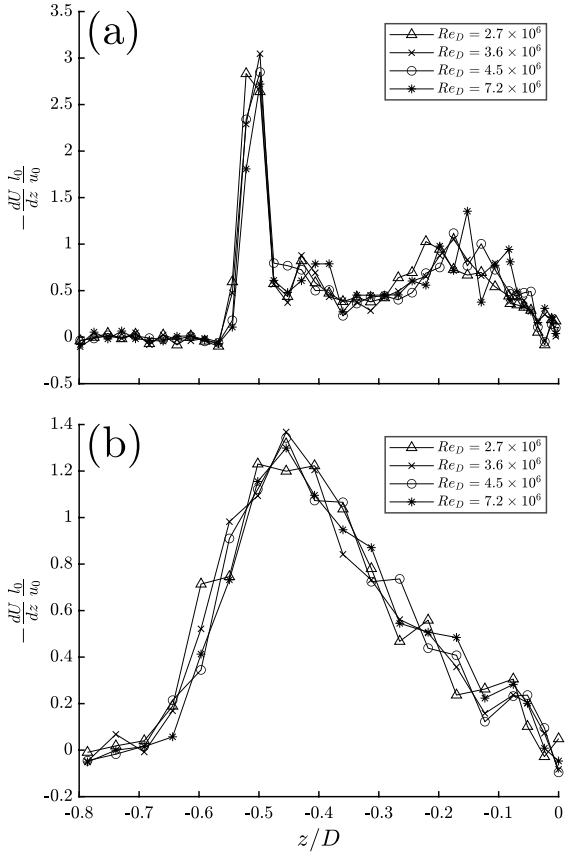

Fig. 10 Spanwise gradients of the axial velocity, $\frac{dU}{dz}$ at $x/D = 0.77$ (a) and $x/D = 3.52$ (b) across half of the wake span ($z/D < 0$) across all Reynolds numbers tested

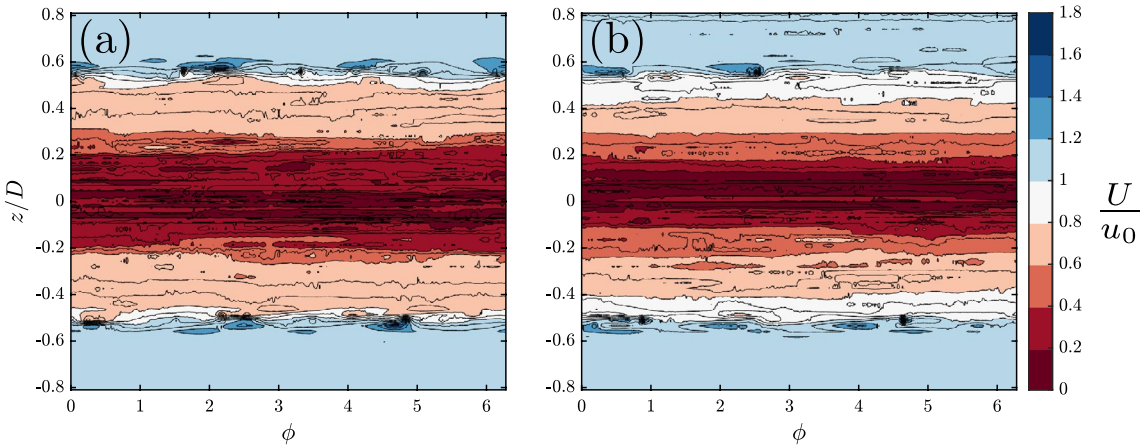

Fig. 9 Phase averaging of axial velocity data at $x/D = 0.77$ and Re_D=2.7×10^6 (a) and 7.2×10^6 (b). The phase averaged period was equal to that of the rotation period of the turbine, i.e., ϕ=2π is equivalent to T_{rot}

To reinforce this hypothesis, the spanwise gradients at $x/D = 3.52$, a position in the intermediate wake, are shown in Fig. 10b as a comparison. At $x/D = 3.52$, no features of the rotor are present, as discussed in Sect. 3.2. The spanwise gradients at this position are more similar to what one would expect for a classical axisymmetric wake, and considering the lack of a local maxima closer to the wake core or edge of Fig. 10b unlike that of Fig. 10a, it is clear that unique near wake features are present in the wake at $x/D = 0.77$. There is no evidence of a Re_D dependence in the spanwise gradients, which supports the findings from Piqué et al. (2020) that found a lack of a Reynolds number dependence for the axial velocity variances across the same range of Re_D.

5 Conclusions

The data presented herein represent one of the highest Reynolds number studies of a wind turbine wake acquired to date and serve as a valuable reference dataset for numerical or analytical efforts at modeling wind turbine wakes. The wake of a horizontal-axis wind turbine was investigated using a high-pressure wind tunnel that enables tests at very high Reynolds numbers. Measurements of the axial velocity were acquired with a nano-scale thermal anemometry probe (NSTAP), to ensure well-resolved data. The data were analyzed to characterize the near and intermediate wake and to identify the transition between the two. Phase averaged results were used to investigate the presence of vortical structures first identified in the variance profiles.

The near wake was determined to persist for about two rotor diameters downstream, where it transitions to the intermediate wake somewhere in the region $2.02 < x/D < 3.52$. The mean velocity deficit profiles exhibited self-similar behavior for all locations tested, except for the most upstream position ($x/D = 0.77$). The far wake, as defined in the classical turbulent shear flow sense, was not observed for any of the downstream distances tested because of the failure of the statistical moments above the first order to obtain self-similarity. Reynolds number effects were determined to be small in all the mean and variance profiles and the mean velocity spanwise gradients. In the wake core of the near wake ($x/D \leq 2.02$), minor Reynolds number effects were observed in the variance profiles of the axial velocity, with a stronger degree of collapse for the lower Re_D case. At the farthest wake position, $x/D = 5.52$, the deficit profiles had a lesser degree of collapse with Reynolds number than the farther upstream positions when nondimensionalized by U_e and D. This observation is likely due to a relative increase in experimental uncertainty due to a decreasing deficit velocity with increasing downstream distance and a difficulty in measuring U_e at the farthest downstream position.

The presence of a self-similar region of the variance profiles in the wake core indicates that discrete root vortices are not present in the wake of the tested turbine model, even at the most upstream location tested. Phase averaged results over the period of the turbine's rotation verified the presence of a shear layer in the wake core rather than discrete root vortices. The self-similar region at the core indicates that the wake core is evolving faster and effectively acts as a wake within the wake which reaches a far-wake state sooner than the outer part. The spanwise gradient of the axial velocity across the wake is found to be independent of Reynolds number, which supports previous findings of Reynolds number invariance for the axial variance in the wake of the same model turbine and across the same Re_D range.

Acknowledgements The authors would like to acknowledge the support of the National Science Foundation under Grant No. CBET 1652583 (Program Manager Ron Joslin).

Author Contributions All authors contributed to the design of the experiment. Material preparation, data collection, and analysis were performed by Alexander Piqué. Measurement stack was designed by Mark A. Miller. The first draft of the manuscript was written by Alexander Piqué. All authors have commented on every manuscript version.

Funding This work was supported by the National Science Foundation under Grant No. CBET 1652583 (Program Manager Ron Joslin).

Availability of data and material The authors report that data will be made available to the public at the following link: https://doi.org/10.34770/1eyw-6f98.

Declarations

Conflicts of interest/Competing interests The authors declare that they have no conflict of interest or competing interests.

Code availability The authors report that there is no relevant code for this submission.

Ethics approval The authors report that no ethics approval was needed for this work.

Consent to participate The authors report that no consent to participate was needed for this work.

Consent for publication The authors report that they have consent for publication.

References

Abraham A, Dasari T, Hong J (2019) Effect of turbine nacelle and tower on the near wake of a utility-scale wind turbine. J Wind Eng Ind Aerodyn 193:103981

Ainslie JF (1988) Calculating the flowfield in the wake of wind turbines. J Wind Eng Indus Aerodynamic 27(1–3):213–224
Bahaj A, Molland A, Chaplin J, Batten W (2007) Power and thrust measurements of marine current turbines under various hydrodynamic flow conditions in a cavitation tunnel and a towing tank. Renew Energ 32(3):407–426
Barthelmie RJ, Jensen L (2010) Evaluation of wind farm efficiency and wind turbine wakes at the Nysted offshore wind farm. Wind Energy 13(6):573–586
Bastankhah M, Porté-Agel F (2014) A new analytical model for wind-turbine wakes. Renew Energy 70:116–123
Butterfield CP, Musial WP, Simms DA (1992) Combined experiment phase I: Final report. Tech. Rep. NREL/TP-257-4655, National Renewable Energy Laboratory
Chamorro LP, Porté-Agel F (2009) A wind-tunnel investigation of wind-turbine wakes: boundary-layer turbulence effects. Bound-Layer Meteorol 132(1):129–149
Chamorro LP, Arndt REA, Sotiropoulos F (2012) Reynolds number dependence of turbulence statistics in the wake of wind turbines. Wind Energy 15(5):733–742
Dairay T, Obligado M, Vassilicos JC (2015) Non-equilibrium scaling laws in axisymmetric turbulent wakes. J Fluid Mech 781:166–195
España G, Aubrun S, Loyer S, Devinant P (2012) Wind tunnel study of the wake meandering downstream of a modelled wind turbine as an effect of large scale turbulent eddies. J Wind Eng Indus Aerodynamic 101:24–33
Fan Y, Arwatz G, Van Buren T, Hoffman D, Hultmark M (2015) Nanoscale sensing devices for turbulence measurements. Exp Fluids 56(7):1–13
Fontaine AA, Straka WA, Meyer RS, Jonson ML, Young SD, Neary VS (2020) Performance and wake flow characterization of a 1: 8.7-scale reference USDOE MHKF1 hydrokinetic turbine to establish a verification and validation test database. Renew Energ 159:451–467
Foti D, Yang X, Guala M, Sotiropoulos F (2016) Wake meandering statistics of a model wind turbine: insights gained by large eddy simulations. Phys Rev Fluids 1(4):044407
Gaumond M, Réthoré PE, Ott S, Peña A, Bechmann A, Hansen KS (2014) Evaluation of the wind direction uncertainty and its impact on wake modeling at the Horns Rev offshore wind farm. Wind Energy 17(8):1169–1178
Howard KB, Singh A, Sotiropoulos F, Guala M (2015) On the statistics of wind turbine wake meandering: an experimental investigation. Phys Fluids 27(7):075103
Howland MF, Bossuyt J, Martínez-Tossas LA, Meyers J, Meneveau C (2016) Wake structure in actuator disk models of wind turbines in yaw under uniform inflow conditions. J Renew Sustainable Energ 8(4):043301
Hutchins N, Monty J, Hultmark M, Smits A (2015) A direct measure of the frequency response of hot-wire anemometers: temporal resolution issues in wall-bounded turbulence. Exp Fluids 56(1):1–18
Iungo GV, Viola F, Camarri S, Porté-Agel F, Gallaire F (2013) Linear stability analysis of wind turbine wakes performed on wind tunnel measurements. J Fluid Mech 737:499–526
Jiménez JM (2007) High Reynolds number flows about bodies of revolution with application to submarines and torpedoes. PhD thesis, Princeton University
Jiménez JM, Hultmark M, Smits AJ (2010) The intermediate wake of a body of revolution at high Reynolds numbers. J Fluid Mech 659:516–539
Johansson PB, George WK, Gourlay MJ (2003) Equilibrium similarity, effects of initial conditions and local Reynolds number on the axisymmetric wake. Phys Fluids 15(3):603–617
Johansson PBV, George WK (2006) The far downstream evolution of the high-Reynolds-number axisymmetric wake behind a disk. Part 1. single-point statistics. J Fluid Mech 555:363–385
Kamada Y, Maeda T, Murata J, Yusuke N (2016) Effect of turbulence on power performance of a horizontal axis wind turbine in yawed and no-yawed flow conditions. Energy 109:703–711
Kang S, Yang X, Sotiropoulos F (2014) On the onset of wake meandering for an axial flow turbine in a turbulent open channel flow. J Fluid Mech 744:376–403
Lin M, Porté-Agel F (2019) Large-eddy simulation of yawed wind-turbine wakes: comparisons with wind tunnel measurements and analytical wake models. Energies 12(23):4574
Lubitz WD (2014) Impact of ambient turbulence on performance of a small wind turbine. Renew Energ 61:69–73
Maeda T, Kamada Y, Murata J, Yonekura S, Ito T, Okawa A, Kogaki T (2011) Wind tunnel study on wind and turbulence intensity profiles in wind turbine wake. J Therm Sci 20(2):127–132
McTavish S, Feszty D, Nitzsche F (2012) An experimental assessment of blockage and Reynolds number effects on wind turbine wake development. Proc of ASME Turbo Expo 2012:949–958
Medici D, Alfredsson P (2006) Measurements on a wind turbine wake: 3d effects and bluff body vortex shedding. Wind Energ 9(3):219–236
Meyers J, Meneveau C (2012) Optimal turbine spacing in fully developed wind farm boundary layers. Wind Energy 15(2):305–317
Miller MA, Kiefer J, Westergaard C, Hansen MOL, Hultmark M (2019) Horizontal axis wind turbine testing at high Reynolds numbers. Phys Rev Fluid 4(11):110504
Neunaber I, Hölling M, Whale J, Peinke J (2021) Comparison of the turbulence in the wakes of an actuator disc and a model wind turbine by higher order statistics: a wind tunnel study. Renew Energ 179:1650–1662
Odemark Y, Fransson JHM (2013) The stability and development of tip and root vortices behind a model wind turbine. Exp Fluids 54:062039. https://doi.org/10.1007/s00348-013-1591-6
Piqué A, Miller MA, Hultmark M (2020) Characterization of the wake behind a horizontal-axis wind turbine (HAWT) at very high Reynolds numbers. J Phys Conf Ser 1618:06203, 062039
Robinson MC, Hand MM, Simms DA, Schreck SJ (1999) Horizontal axis wind turbine aerodynamics: Three-dimensional, unsteady, and separated flow influences. Tech. Rep. NREL/CP-500-26337, National Renewable Energy, Laboratory
Sforza P, Sheerin P, Smorto M (1981) Three-dimensional wakes of simulated wind turbines. AIAA J 19(9):1101–1107
Simms D, Schreck S, Hand M, Fingersh LJ (2001) NREL unsteady aerodynamics experiment in the NASA-Ames wind tunnel: a comparison of predictions to measurements. Tech. Rep. NREL/TP-500-29494, 783409, National Renewable Energy Laboratory
Snel H, Schepers JG, Montgomerie B (2007) The MEXICO project (model experiments in controlled conditions): The database and first results of data processing and interpretation. J Phys: Conf Ser 75:012014
Sonnenberger R, Graichen K, Erk PFourier averaging: a phase-averaging method for periodic flow. Exp Fluids 28(3): 217–224
Sørensen JN, Shen WZ, Munduate X (1998) Analysis of wake states by a full-field actuator disc model. Wind Energy 1(2):73–88
alavera M, Shu F, (2017) Experimental study of turbulence intensity influence on wind turbine performance and wake recovery in a low-speed wind tunnel. Renew Energ 109:363–371
Townsend AA (1956) The structure of turbulent shear flow. Cambridge University Press, London
Uberoi MS, Freymuth P (1970) Turbulent energy balance and spectra of the axisymmetric wake. Phys Fluids 13(9):2205–2210

Vallikivi M, Hultmark M, Bailey SCC, Smits AJ (2011) Turbulence measurements in pipe flow using a nano-scale thermal anemometry probe. Exp Fluids 51(6):1521–1527

Vermeer LJ, Sørensen JN, Crespo A (2003) Wind turbine wake aerodynamics. Prog Aerosp Sci 39(6–7):467–510

Wang C, Campagnolo F, Canet H, Barreiro DJ, Bottasso CL (2021) How realistic are the wakes of scaled wind turbine models? Wind Energ Sci 6(3):961–981

Zhang W, Markfort CD, Porté-Agel F (2013) Wind-turbine wakes in a convective boundary layer: a wind-tunnel study. Bound-Layer Meteorol 146(2):161–179

Zhao X, Hu T, Zhang L, Liu Z, Wang S, Tian W, Yang Z, Guo Y (2021) Experimental study on the characteristics of wind turbine wake field considering yaw conditions. Energ Sci & Eng 9(12):2333–2341

Publisher's Note Springer Nature remains neutral with regard to jurisdictional claims in published maps and institutional affiliations.